

# Generic constraints on the Relativistic Mean-Field and Skyrme-Hartree-Fock models from the pure neutron matter equation of state

F. J. Fattoyev,<sup>1,2,\*</sup> W. G. Newton,<sup>1,†</sup> Jun Xu,<sup>1,‡</sup> and Bao-An Li<sup>1,§</sup>

<sup>1</sup>*Department of Physics and Astronomy, Texas A&M University-Commerce, Commerce, Texas 75429-3011, USA*

<sup>2</sup>*Institute of Nuclear Physics, Tashkent 100214, Uzbekistan*

(Dated: April 3, 2024)

We study the nuclear symmetry energy  $S(\rho)$  and related quantities of nuclear physics and nuclear astrophysics predicted *generically* by relativistic mean-field (RMF) and Skyrme-Hartree-Fock (SHF) models. We establish a simple prescription for preparing equivalent RMF and SHF parameterizations starting from a minimal set of empirical constraints on symmetric nuclear matter, nuclear binding energy and charge radii, enforcing equivalence of their Lorenz effective masses, and then using the pure neutron matter (PNM) equation of state (EoS) obtained from *ab-initio* calculations to optimize the pure isovector parameters in the RMF and SHF models. We find the resulting RMF and SHF parameterizations give broadly consistent predictions of the symmetry energy  $J$  and its slope parameter  $L$  at saturation density within a tight range of  $\lesssim 2$  MeV and  $\lesssim 6$  MeV respectively, but that clear model dependence shows up in the predictions of higher-order symmetry energy parameters, leading to important differences in (a) the slope of the correlation between  $J$  and  $L$  from the confidence ellipse, (b) the isospin-dependent part of the incompressibility of nuclear matter  $K_\tau$ , (c) the symmetry energy at supra-saturation densities, and (d) the predicted neutron star radii. The model dependence can lead to about 1-2 km difference in predictions of the neutron star radius given *identical* predicted values of  $J$ ,  $L$  and symmetric nuclear matter (SNM) saturation properties. Allowing the full freedom in the effective masses in both models leads to constraints of  $30 \lesssim J \lesssim 31.5$  MeV,  $35 \lesssim L \lesssim 60$  MeV,  $-330 \lesssim K_\tau \lesssim -216$  MeV for the RMF model as a whole and  $30 \lesssim J \lesssim 33$  MeV,  $28 \lesssim L \lesssim 65$  MeV,  $-420 \lesssim K_\tau \lesssim -325$  MeV for the SHF model as a whole. Notably, given PNM constraints, these results place RMF and SHF models *as a whole* at odds with some constraints on  $K_\tau$  inferred from giant monopole resonance and neutron skin experimental results.

PACS numbers: 21.65.Cd, 21.65.Mn, 26.60.Kp, 26.60.-c

## I. INTRODUCTION

Highly isospin asymmetric nuclear matter is present in heavy nuclei far from the stability line and in the surface regions of nuclei exhibiting neutron skins and occurs during heavy-ion collisions and also in astrophysical systems such as neutron stars. Its energy relative to that of symmetric nuclear matter (SNM) is usefully characterized by the symmetry energy as a function of density  $S(\rho)$ , and therefore the constraining of  $S(\rho)$ , particularly at densities away from nuclear saturation density  $\rho_0$ , has been the subject of much recent experimental and theoretical activity [1–19]. Particularly, constraints extracted for the magnitude of the symmetry energy at saturation density  $J \equiv S(\rho_0)$  and its slope there  $L$  span the ranges  $J \approx 25 - 35$  MeV and  $L \approx 25 - 115$  MeV although the  $J$  constraints from mass models alone are much tighter, and most recent  $L$  constraints are placed in the range  $30 - 80$  MeV (see, e.g., [19] and Fig. 1 from [20]). Extraction of such constraints requires specifying a model for nucleon-nucleon interactions which tends to be equivalent to specifying a choice of functional form for  $S(\rho)$  in the RMF and SHF models. It is the influence of such choices on predictions of symmetry energy and simple, related, nuclear and astrophysical properties that will be the subject of this paper.

Given the currently prohibitive complexity of computing the nucleon-nucleon (NN) interaction from the underlying theory of QCD and the challenges of solving the nuclear many-body problems, progress in nuclear many-body theory has developed along two lines:

(1) The microscopic approach builds up the many body system from bare NN interactions together with a usually phenomenological description of the three-nucleon (3N) interaction; in-medium correlations are self-consistently in-

\*Electronic address: Farrooh.Fattoyev@tamuc.edu

†Electronic address: William.Newton@tamuc.edu

‡Electronic address: Jun.Xu@tamuc.edu

§Electronic address: Bao-An.Li@tamuc.edu

cluded via the many-body calculational technique. In the last few years, much theoretical progress in understanding neutron-rich systems has been accomplished through microscopic pure neutron matter (PNM) calculations. By studying the universal behavior of resonant Fermi gases with infinite scattering length, a significant constraint is achieved for the equation of state of dilute neutron matter [21]. These calculations have been extended to higher densities using the full power of Quantum Monte Carlo methods [22, 23]. By studying the physics of chiral three-nucleon forces the EoS of PNM is obtained perturbatively up to nuclear saturation density [24]. Finally, the Auxiliary Field Diffusion Monte Carlo (AFDMC) technique, which takes into account the realistic nuclear Hamiltonian containing modern two- and three-body interactions of the Argonne potential and Urbana family of three-body nucleon forces, has been used to calculate the EoS of PNM up to and above saturation density [25–27]. The outcome of the above investigations is a robust prediction for the EoS of PNM at low densities where only two body interactions are important, and a systematic investigation of the uncertainties in the EoS of PNM up to and beyond saturation density as a result of our present uncertainties in the three-neutron interaction, resulting in “theoretical error bars” in that density regime.

(2) The second approach is to construct an effective interaction describing the *in-medium* nucleon-nucleon interaction, subject to most of the symmetries of the bare potential. The effective interaction is typically dependent on  $\sim 10$  parameters representing, for example, coupling constants, which are fit to experimental data sets from finite nuclei properties such as binding energies, charge radii, single particle energy spectra and spectra of collective excitations. One of the overriding goals of modern nuclear many-body theory is to derive an energy-density functional (EDF) [28] with clear physical connections to *ab initio* NN interactions and QCD. The widely used RMF [29, 30] and SHF [31, 32] models, with the latter thought of as a non-relativistic expansion of the former [33, 34], are two typical phenomenological EDFs used in nuclear many-body theory. Both models have  $\lesssim 10$  free parameters in their simplest forms. Recent surveys find about 240 parameter sets for the SHF model [35] and 10s of parameterizations of the simplest form of the RMF model, e.g. [36], although many are old parameter sets superseded by parameter sets fit to more recent, accurate data. We shall refer to the space inhabited by the free parameters as the model space, and the two classes of EDF (RMF and SHF) shall be referred to as the two models. Since the number of experimental observables is always larger than the number of free parameters, the problem of optimizing these EDFs is always overdetermined, and this results in a considerable degeneracy amongst parameter sets, and correlations between individual parameters when constrained by certain observables. Covariance analysis techniques [37, 38] have been employed to study correlations between predicted observables from a particular EDF in its model space. Given a certain experimental constraint, this analysis method serves as a useful tool to optimize the parameters of RMF and SHF EDFs and systematically examine the correlations between various nuclear matter and neutron star properties [16].

Most parameterizations of EDFs are obtained through fitting to predominantly nuclear experimental data sets, thus probing closely isospin symmetric systems; their predictions of symmetry energy behaviors thus vary widely, and many do not give PNM predictions consistent with microscopic calculations. Recent parameterizations which do take into account *ab-initio* PNM calculations tend to give behaviors of the symmetry energy at odds with some experimental constraints from giant monopole resonances and neutron skins [7, 39, 40]; constraints extracted, in part, using the same types of EDFs. This discrepancy also occurs in microscopic calculations [41]. This raises questions such as: can such discrepancies be resolved by choosing a different parameterization? Are the extracted constraints correct? Is there a fundamental problem with the particular EDFs used? A systematic study of *parameterization-independent* RMF and SHF model predictions of the behavior of  $J$  and  $L$  and related physical properties has yet to be undertaken.

RMF and SHF models predict different functional forms for  $S(\rho)$  and thus one might expect generic differences in the values extracted from the same sets of data within each model, and conversely, generic differences in the predictions of properties of neutron-rich systems, even given the same values of  $J$  and  $L$ . This potentially makes combining the two types of functional in modeling experimental phenomena hazardous; it also means that extraction of, for example, constraints on  $J$  and  $L$  from nuclear experiment or astrophysical observation (e.g. the measurement of neutron star radii) comes with the caveat that such constraints are dependent on the model used for extraction. It is important to attempt to quantify what difference that model choice makes.

The aim of this paper is to explore the generic predictions of properties of isospin-asymmetric nuclear matter from RMF and SHF EDFs simultaneously constrained by the best theoretical knowledge of the PNM EoS. Particularly, we will set model-generic best fit values and  $1\sigma$  confidence intervals on  $J$ ,  $L$ ,  $K_\tau$  and neutron skin thicknesses arising from the optimization to the theoretical PNM EoS; we will examine whether the discrepancies between the predicted values of  $K_\tau$  and those extracted from experiment are endemic to the two EDFs as a whole, and we will explore the model dependence of the above results, the supra-saturation symmetry energy and neutron star properties arising from the different functional forms of the two models. We should note here that our aim is neither to establish new parameterizations of either model, nor to set absolute constraints on symmetry energy, but to explore as far as possible the *generic* constraints that can be placed by each model on neutron-rich systems once constrained by information from the PNM EoS.

The manuscript is organized as follows. In Sec. II we briefly review the two EDFs and the covariance analysis method used to optimize the two pure isovector parameters in the EDFs. Results are presented in Sec. III and in

Sec. IV we conclude.

## II. FORMALISM

To ease discussions, we recall in this section the main formulas related to the symmetry energy, the RMF and SHF models, and the covariance analysis method used to examine the effect of the PNM constraints on the two models.

### A. Symmetry energy

The binding energy per nucleon in neutron-rich nuclear matter can be written as

$$E(\rho, \alpha) = E_0(\rho) + S(\rho)\alpha^2 + \mathcal{O}(\alpha^4), \quad (1)$$

where  $\rho$  is the baryon number density and  $\alpha = (\rho_n - \rho_p)/\rho$  is the isospin asymmetry, with  $\rho_n(\rho_p)$  being the neutron (proton) number density. Around the saturation density  $\rho_0$ , the symmetry energy can be expressed as

$$S(\rho) = J + L\chi + \frac{1}{2}K_{\text{sym}}\chi^2 + \mathcal{O}(\chi^3), \quad (2)$$

where  $\chi \equiv (\rho - \rho_0)/3\rho_0$ ,  $J$  is the value of the symmetry energy at saturation density,  $L$  is the slope parameter, and  $K_{\text{sym}}$  is the curvature parameter at saturation density given, respectively, by the following expressions:

$$L = 3\rho_0 \left( \frac{\partial S(\rho)}{\partial \rho} \right)_{\rho=\rho_0}, \quad (3)$$

$$K_{\text{sym}} = 9\rho_0^2 \left( \frac{\partial^2 S(\rho)}{\partial \rho^2} \right)_{\rho=\rho_0}. \quad (4)$$

The coefficients of the higher-order terms in Eq. (1) are generally much smaller than  $S(\rho)$ , so it is usually a good approximation to write the energy per nucleon in PNM as  $E_{\text{PNM}}(\rho) \approx E_0(\rho) + S(\rho)$ ; however, in this work we calculate  $E_{\text{PNM}}$  using the full EoS.

### B. Relativistic mean-field model

The commonly employed RMF model contains an isodoublet nucleon field ( $\psi$ ) interacting via the exchange of the scalar-isoscalar  $\sigma$ -meson ( $\phi$ ), the vector-isoscalar  $\omega$ -meson ( $V^\mu$ ), the vector-isovector  $\rho$ -meson ( $\mathbf{b}^\mu$ ), and the photon ( $A^\mu$ ) [29, 30, 42]. The effective Lagrangian density for the model can be written as

$$\begin{aligned} \mathcal{L} = & \bar{\psi} \left[ \gamma^\mu \left( i\partial_\mu - g_\sigma V_\mu - \frac{g_\rho}{2} \boldsymbol{\tau} \cdot \mathbf{b}_\mu - \frac{e}{2} (1 + \tau_3) A_\mu \right) - (M - g_s \phi) \right] \psi + \frac{1}{2} \partial_\mu \phi \partial^\mu \phi - \frac{1}{2} m_s^2 \phi^2 \\ & - \frac{1}{4} V^{\mu\nu} V_{\mu\nu} + \frac{1}{2} m_v^2 V^\mu V_\mu - \frac{1}{4} \mathbf{b}^{\mu\nu} \cdot \mathbf{b}_{\mu\nu} + \frac{1}{2} m_\rho^2 \mathbf{b}^\mu \cdot \mathbf{b}_\mu - \frac{1}{4} F^{\mu\nu} F_{\mu\nu} - U(\phi, V_\mu, \mathbf{b}_\mu), \end{aligned} \quad (5)$$

where  $V_{\mu\nu}$ ,  $\mathbf{b}_{\mu\nu}$ , and  $F_{\mu\nu}$  are the isoscalar, isovector, and electromagnetic field tensors, respectively:

$$V_{\mu\nu} = \partial_\mu V_\nu - \partial_\nu V_\mu, \quad (6a)$$

$$\mathbf{b}_{\mu\nu} = \partial_\mu \mathbf{b}_\nu - \partial_\nu \mathbf{b}_\mu, \quad (6b)$$

$$F_{\mu\nu} = \partial_\mu A_\nu - \partial_\nu A_\mu. \quad (6c)$$

The nucleon mass  $M$  and meson masses  $m_s$ ,  $m_v$ , and  $m_\rho$  may be treated as empirical parameters. The effective potential  $U(\phi, V_\mu, \mathbf{b}_\mu)$  consists of non-linear meson interactions that simulates the complicated dynamics encoded in just few model parameters. In the present work we use the following form of the effective potential [43]:

$$U(\phi, V^\mu, \mathbf{b}^\mu) = \frac{\kappa}{3!} (g_s \phi)^3 + \frac{\lambda}{4!} (g_s \phi)^4 - \frac{\zeta}{4!} g_v^4 (V_\mu V^\mu)^2 - \Lambda_v g_\rho^2 \mathbf{b}_\mu \cdot \mathbf{b}^\mu g_v^2 V_\nu V^\nu. \quad (7)$$

This model is described by 7 interaction parameters:  $\{g_s, g_v, g_\rho, \kappa, \lambda, \zeta, \Lambda_v\}$ . Note that power counting suggests that a consistent Lagrangian density should include all terms up to fourth order in the meson fields. However, the existing database of both laboratory and observational data appears to be accurately described by the the minimal set of parameters [43–45]. Indeed, it was shown that ignoring a subset of model parameters that are of the same order in a power-counting scheme does not compromise the quality of the fit [42, 46].

### C. Skyrme-Hartree-Fock model

The standard form of the energy density obtained from the zero-range Skyrme interaction using the Hartree-Fock method can be written as [47]

$$\begin{aligned}
\mathcal{H} = & \frac{\hbar^2}{2M} \tau + t_0 [(2+x_0)\rho^2 - (2x_0+1)(\rho_n^2 + \rho_p^2)]/4 \\
& + t_3 \rho^\sigma [(2+x_3)\rho^2 - (2x_3+1)(\rho_n^2 + \rho_p^2)]/24 \\
& + [t_2(2x_2+1) - t_1(2x_1+1)](\tau_n \rho_n + \tau_p \rho_p)/8 + [t_1(2+x_1) + t_2(2+x_2)]\tau\rho/8 \\
& + [3t_1(2+x_1) - t_2(2+x_2)](\nabla\rho)^2/32 - [3t_1(2x_1+1) + t_2(2x_2+1)][(\nabla\rho_n)^2 + (\nabla\rho_p)^2]/32 \\
& + W_0 [\vec{J} \cdot \nabla\rho + \vec{J}_n \cdot \nabla\rho_n + \vec{J}_p \cdot \nabla\rho_p]/2 + (t_1 - t_2)[J_n^2 + J_p^2]/16 - (t_1 x_1 + t_2 x_2)J^2/16.
\end{aligned} \tag{8}$$

Here  $\rho_q$ ,  $\tau_q$ , and  $\vec{J}_q$  ( $q = p, n$ ) are, respectively, the number, kinetic, and spin-current densities, and  $\rho$ ,  $\tau$ , and  $\vec{J}$  are the corresponding total densities. The SHF model is expressed in terms of 9 Skyrme parameters:  $\{t_0, t_1, t_2, t_3, x_0, x_1, x_2, x_3, \sigma\}$  and the spin-orbit coupling constant  $W_0$  which is taken as 133.3 MeV fm<sup>5</sup> [10] in the present work.

### D. Covariance analysis method

Here we very briefly discuss the covariance analysis method used in the present work. For more details, we refer the readers to Refs. [37, 38, 48]. Given a set of  $N$  experimental observables  $\mathcal{O}_n^{(\text{exp})}$  that are determined with an accuracy of  $\Delta\mathcal{O}_n$ , one can minimize the quality measure  $\chi^2$ :

$$\chi^2(\mathbf{p}) \equiv \sum_{n=1}^N \left( \frac{\mathcal{O}_n^{(\text{th})}(\mathbf{p}) - \mathcal{O}_n^{(\text{exp})}}{\Delta\mathcal{O}_n} \right)^2. \tag{9}$$

Here each of the  $N$  observables is computed within the given model  $\mathcal{O}_n^{(\text{th})}(\mathbf{p})$  as a function of the  $F$  model parameters  $\mathbf{p} = (p_1, \dots, p_F)$ . A set of optimal parameters  $\mathbf{p}_0$  are determined via a least square fit to the quality measure. For our set of ‘experimental’ observables  $\mathcal{O}_n^{(\text{exp})}$  in the  $\chi^2$  input we choose the theoretical calculations of the energy per neutron  $E_{\text{PNM}}$  in the density range of  $0.04 \leq \rho \leq 0.16 \text{ fm}^{-3}$  [24, 25, 49]. Although the AFDMC calculations have been extended up to several times the saturation density [27], the extension of the calculations of the chiral three-nucleon forces to higher densities using piecewise polytropes [50] shows that the uncertainties in the EoS could be very large when all of these models are employed. Therefore we rely on the PNM calculations that are obtained up to saturation density only. Moreover, the symmetry energy coefficients are only sensitive to the equation of state around the saturation density.

Once the optimal parameter set  $\mathbf{p}_0$  is found through the  $\chi^2$ -minimization, one can then compute and diagonalize the symmetric matrix of second derivatives. All the information about the behavior of the  $\chi^2$  function around the minimum is contained in this matrix. That is,

$$\chi^2(\mathbf{p}) - \chi^2(\mathbf{p}_0) \equiv \Delta\chi^2(\mathbf{x}) = \mathbf{x}^T \hat{\mathcal{M}} \mathbf{x} = \boldsymbol{\xi}^T \hat{\mathcal{D}} \boldsymbol{\xi} = \sum_{i=1}^F \lambda_i \xi_i^2, \tag{10}$$

where

$$x_i \equiv \frac{(\mathbf{p} - \mathbf{p}_0)_i}{(\mathbf{p}_0)_i} \tag{11}$$

are scaled dimensionless variables,  $\hat{\mathcal{M}} = \hat{\mathcal{A}} \hat{\mathcal{D}} \hat{\mathcal{A}}^T$ , and  $\boldsymbol{\xi} = \hat{\mathcal{A}}^T \mathbf{x}$  are dimensionless variables in a rotated basis. Here  $\hat{\mathcal{A}}$  is the orthogonal matrix whose columns are composed of the normalized eigenvectors and  $\hat{\mathcal{D}} = \text{diag}(\lambda_1, \dots, \lambda_F)$  is the diagonal matrix of eigenvalues. The meaningful theoretical uncertainties can be obtained by computing the statistical covariance of two observables  $A$  and  $B$  which can be written as follows:

$$\text{cov}(A, B) = \sum_{i,j=1}^F \frac{\partial A}{\partial x_i} (\hat{\mathcal{M}}^{-1})_{ij} \frac{\partial B}{\partial x_j} = \sum_{i=1}^F \frac{\partial A}{\partial \xi_i} \lambda_i^{-1} \frac{\partial B}{\partial \xi_i}. \tag{12}$$

The variance  $\sigma^2(A)$  of a given observable  $A$  is then simply given by  $\sigma^2(A) = \text{cov}(A, A)$ . Finally, the covariance ellipses between two observables  $A$  and  $B$  can be plotted by diagonalizing the  $2 \times 2$  covariance matrix:

$$\hat{C} = \begin{pmatrix} \text{cov}(A, A) & \text{cov}(A, B) \\ \text{cov}(B, A) & \text{cov}(B, B) \end{pmatrix} \quad (13)$$

Then the eigenvalues of this matrix represent the semi-major and semi-minor axes of the covariance ellipse, while the eigenvectors provide the orientation of the ellipse.

### III. RESULTS

Following the idea of building relations between values of model parameters and macroscopic nuclear quantities [10], one finds that by changing the two solely isovector parameters, which are  $g_\rho$  and  $\Lambda_v$  in the RMF model [51], and  $x_0$  and  $x_3$  in the SHF model, only the symmetry energy  $S(\rho)$  is modified while properties of SNM such as saturation density  $\rho_0$ , binding energy per nucleon at saturation density  $E_0$ , incompressibility coefficient at saturation density  $K_0$ , and effective mass  $M^*$  at saturation all remain unchanged. Thus, in the following we optimize the two isovector parameters [ $F = 2$  in Eqs. (10) and (12)] with respect to the available range of PNM EoSs to constrain the values of  $J$  and  $L$  at saturation density by employing the covariance analysis method discussed above.

#### A. Reference models

As representative RMF parameterizations, we choose the accurately-calibrated NL3\* [52] and the recent IU-FSU [53] parameterizations. The IU-FSU is the recent parameterization that was validated against experimental, observational, and theoretical data, while the accurately-calibrated NL3\* parameterization gives a much stiffer EoS of SNM (larger value of  $K_0$  and smaller value of  $\zeta$  parameter) and a stiff symmetry energy (larger values of symmetry energy  $J$  and slope  $L$ ) and therefore offers a suitable contrast to IU-FSU.

To compare the RMF and SHF models on the same footing, we create two Skyrme parameterizations which give the same properties of nuclear matter at saturation as the two RMF parameterizations, herein referred to as SkNL3\* and SkIU-FSU forces, through the method of writing the Skyrme parameters as functions of macroscopic nuclear quantities [10, 54]. Note that these two new Skyrme parameterizations are intended only to serve as references in this study.

Several definitions of the nucleon effective mass exist in the literature [55]. In the RMF model the Dirac effective mass is defined through the scalar part of the nucleon self-energy in the Dirac equation:

$$M_{D,q}^* = M_q + \Sigma_q^s, \quad (14)$$

where the nucleon self-energy is given as  $\Sigma_n^s \equiv \Sigma_p^s = -g_s \phi$  in the RMF model considered in this work. It has been well documented that there is a strong correlation between the Dirac effective nucleon mass at saturation density  $M_D^*$  and the strength of the spin-orbit force in nuclei [30, 33, 56, 57]. Indeed, one of the most compelling features of RMF models is the reproduction of the spin-orbit splittings in finite nuclei. This occurs when the velocity dependence of the equivalent central potential that leads to saturation arises primarily due to a reduced nucleon effective mass [58]. It is shown that models with effective masses outside the range  $0.58 < M_D^*/M < 0.64$  will not be able to reproduce empirical spin-orbit couplings [58], when no tensor couplings are taken into account. On the other hand, the non-relativistic effective mass parameterizes the momentum dependence of the single particle potential, which is the result of a quadratic parameterization of the single particle spectrum. A recent study [35] puts a bound of  $0.69 < M^*/M < 1.0$  for the non-relativistic effective masses. It has been argued [59] that the so-called Lorentz mass  $M_L^*$  should be compared with the non-relativistic effective mass extracted from analyses carried out in the framework of nonrelativistic optical and shell models. For consistency, we choose the effective mass in the Skyrme parameterizations to be equal to the Lorentz mass in the RMF parameterizations. Since the RMF model we use in this work gives the same isoscalar and isovector effective masses, we set them equal in the reference SHF model too.

Finally, the isoscalar parameters of the two reference Skyrme forces are then re-adjusted to fit the binding energy and charge radius of  $^{208}\text{Pb}$  by adjusting only the saturation density  $\rho_0$  and the binding energy  $E_0$  of SNM. As shown in Fig. 1, these models predict the charge radii and binding energies of other doubly closed-shell nuclides within 1-2% accuracy. We note that these finite nuclei properties are obtained by solving the Dirac equation for the RMF model and the Schrödinger equation for the SHF model. The bulk nuclear matter observables predicted by these reference models are given in Table I. In terms of the predicted values of isoscalar and isovector bulk observables, both corresponding RMF and SHF models are therefore almost equivalent.

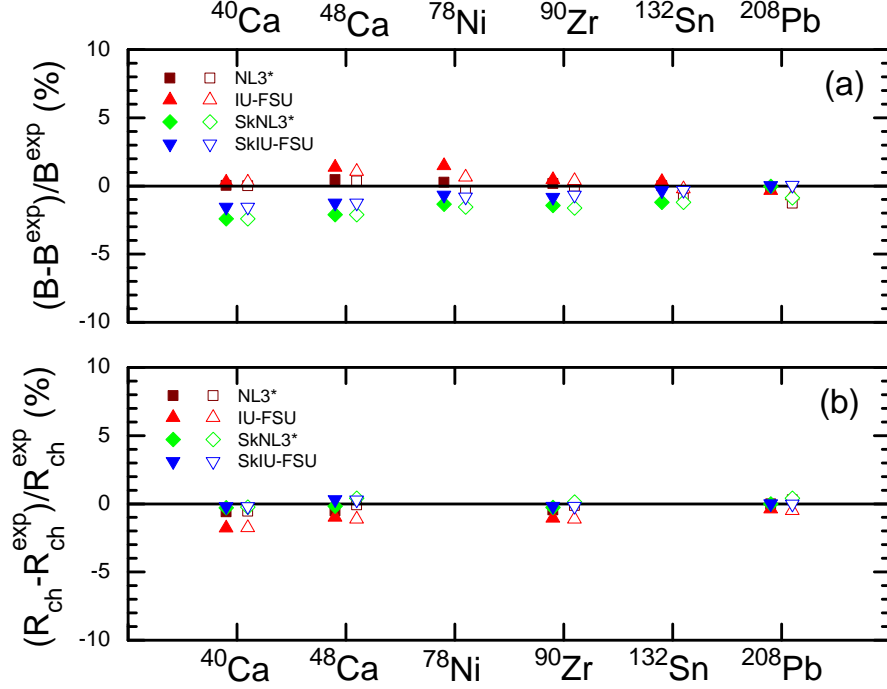


FIG. 1: (Color online) Relative deviation of the binding energies (a) and charge radii (b) of closed-shell nuclei from the reference models discussed in the text compared with the experimental data (with superscript ‘exp’) from Refs. [60, 61]. Filled symbols are from the original parameterizations and empty symbols are from the PNM modified parameterizations.

	$\rho_0$ (fm $^{-3}$ )	$E_0$ (MeV)	$K_0$ (MeV)	$M_D^*$ (M)	$M_L^*$ (M)	$M_S^*$ (M)	$M_V^*$ (M)	$J$ (MeV)	$L$ (MeV)	$K_{\text{sym}}$ (MeV)	$R_{\text{skin}}$ (fm)
NL3*	0.1500	-16.32	258.49	0.594	0.671	-	-	38.7	122.7	105.7	0.29
SkNL3*	0.1527	-15.76	258.49	-	-	0.671	0.671	38.7	122.7	62.7	0.27
IU-FSU	0.1546	-16.40	231.33	0.609	0.687	-	-	31.3	47.2	28.5	0.16
SkIU-FSU	0.1575	-15.70	231.33	-	-	0.687	0.687	31.3	47.2	-132.0	0.16

TABLE I: Macroscopic quantities from four reference parameterizations. They are binding energy per nucleon  $E_0$  and incompressibility  $K_0$  of SNM, Dirac ( $M_D^*$ ) and Lorentz ( $M_L^*$ ) effective mass from the RMF model, non-relativistic isoscalar ( $M_S^*$ ) and isovector ( $M_V^*$ ) effective mass from the SHF model, the symmetry energy  $J$ , its slope parameter  $L$  and curvature parameter  $K_{\text{sym}}$  at saturation density, and the resulting neutron skin thickness  $R_{\text{skin}}$  of  $^{208}\text{Pb}$ .

The energy per neutron  $E_{\text{PNM}}$  predictions at sub-saturation densities for our reference models are plotted on the left panel (a) of Fig. 2, compared to the results obtained by various microscopic approaches. One can see that even among our four parameterizations there is wide variance in the EoS of PNM at all densities, and little agreement with those microscopic calculations. The very wide range of predictions of the symmetry energy parameters and the corresponding widespread predictions for the neutron skins of nuclei inherent in these parameterizations are seen in Table I.

## B. Symmetry Energy Coefficients

Having established our reference models, we next minimize the  $\chi^2$  with respect to the PNM constraints [24, 27, 49] in the density range of  $0.04 \leq \rho \leq 0.16$  fm $^{-3}$  by adjusting two isolated (solely isovector) parameters. This leads to optimized values of the model parameters and thus the density dependence of symmetry energy up to saturation density once the EoS of SNM is fixed. All isoscalar parameters remain unchanged and there is very little change in the prediction of binding energies and charge radii as is shown in Fig. 1.

As can be seen in panel (b) of Fig. 2, we obtain the EoS of PNM for a given RMF or SHF parameterization that best fits within the band of microscopic PNM calculations at the minimum of the  $\chi^2$ -function. The resulting RMF and

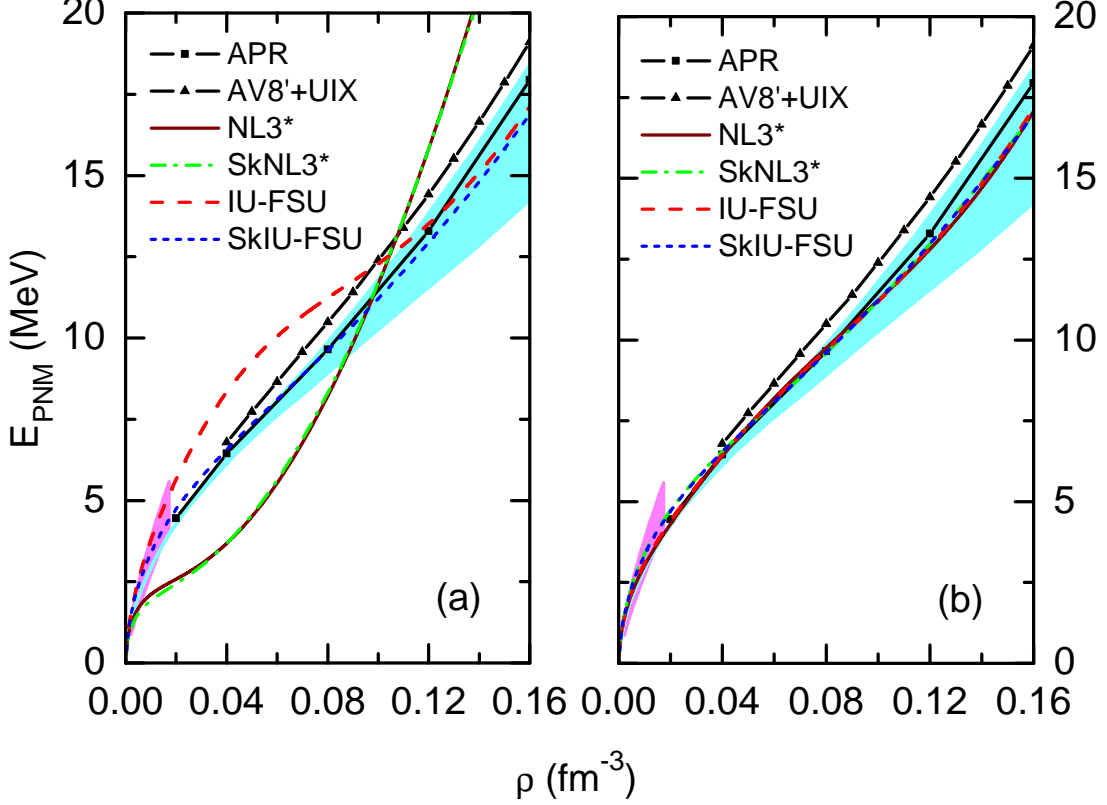


FIG. 2: (Color online) Comparing the PNM EoS from four reference parameterizations with the AFDMC EoS in the AV8'+UIX Hamiltonian [27], the variational APR EoS [49], the low-density band from the constraints of resonant Fermi gases [21], and the high-density band from the chiral effective field theory calculations with 3-neutron forces [24], before (a) and after (b) PNM optimization.

	$S_{0.1}^0$	$S_{0.1}$	$J^0$	$J$	$L^0$	$L$	$K_{\text{sym}}^0$	$K_{\text{sym}}$	$K_{\tau}^0$	$K_{\tau}$	$R_{\text{skin}}^0$	$R_{\text{skin}}$
NL3*	25.7	$24.9 \pm 0.4$	38.7	$30.7 \pm 0.7$	122.7	$50.3 \pm 1.8$	105.7	$39.2 \pm 17.8$	-684.4	$-284.6 \pm 29.4$	0.29	$0.18 \pm 0.01$
SkNL3*	25.0	$24.5 \pm 0.3$	38.7	$31.0 \pm 0.9$	122.7	$46.4 \pm 6.4$	62.7	$-156.0 \pm 16.6$	-529.4	$-380.0 \pm 15.2$	0.27	$0.16 \pm 0.01$
IU-FSU	25.7	$24.9 \pm 0.4$	31.3	$31.4 \pm 0.7$	47.2	$52.9 \pm 2.0$	28.5	$-6.8 \pm 12.9$	-195.3	$-257.6 \pm 22.3$	0.16	$0.18 \pm 0.01$
SkIU-FSU	24.4	$24.4 \pm 0.3$	31.3	$31.4 \pm 0.9$	47.2	$48.0 \pm 6.2$	-132.0	$-130.2 \pm 13.3$	-343.9	$-345.6 \pm 15.3$	0.16	$0.16 \pm 0.01$

TABLE II: Isovector observables and associated  $1\sigma$  error bars from four reference parameterizations before (with superscript '0') and after (without superscript '0') the PNM constraints are applied. Values are shown for the symmetry energy at  $\rho = 0.1 \text{ fm}^{-3}$   $S_{0.1}$  and at saturation density  $J$ , slope parameter  $L$ , curvature parameter  $K_{\text{sym}}$ , isospin-dependent part of incompressibility  $K_{\tau}$ , and the neutron skin thickness  $R_{\text{skin}}$  of  $^{208}\text{Pb}$ . All the quantities are in MeV apart from  $R_{\text{skin}}$  which is in fm.

SHF models predict very similar symmetry energies  $J$ , while the RMF model predicts a consistently higher central value for  $L$  by about 4-5 MeV than the SHF model as shown in Table II.

The  $1\sigma$  errors on these two isolated parameters can be translated into equivalent errors on  $J$  and  $L$ . The errors in  $J$  are less than  $\pm 1$  MeV for all the parameterizations. The RMF model gives a relatively small error in  $L$  of around  $\pm 2$  MeV, while the SHF model gives a much larger error around  $\pm 6$  MeV. Table II appears to indicate that within the  $1\sigma$  errors, both models are consistent in their predicted values of  $J$  and  $L$ . However, in Fig. 3 we plot a  $1\sigma$  joint confidence regions in the  $J$ - $L$  plane for both RMF and SHF models, thus showing that in fact the two models predict non-overlapping regions in  $J$ - $L$  space. Both models show a positive correlation between  $J$  and  $L$ , but with differing slopes. For example, for IU-FSU and SkIU-FSU parameterizations the relations are approximately

$$\begin{aligned} L &= (2.4 J - 23) \text{ MeV}, & (\text{RMF}) \\ L &= (6.0 J - 140) \text{ MeV}, & (\text{SHF}) \end{aligned} \quad (15)$$

within the constraints of  $J$  and  $L$  shown in Table II.

The origin of this difference lies mainly in the values of the higher-order symmetry energy parameters that are predicted upon optimization. There is a strong model dependency in the prediction for the curvature parameter of the symmetry energy  $K_{\text{sym}}$  (see Table II). For example, after the PNM optimization IU-FSU predicts  $K_{\text{sym}} = -6.8 \pm 12.9$  MeV, while its Skyrme-like version predicts a smaller value of  $K_{\text{sym}} = -130.2 \pm 13.3$  MeV. When we plot the  $1\sigma$  joint confidence regions in the  $K_{\text{sym}}-L$  plane for both RMF and SHF models (see the left panel (a) of Fig. 4) further differences can be seen: there is, generically, a negative correlation between the slope of the symmetry energy and  $K_{\text{sym}}$  in the RMF model, while this correlation is positive in the case of the SHF model. Only at a sub-saturation density of  $\rho = 0.1 \text{ fm}^{-3}$  do the two models have similar values of  $K_{\text{sym}}$  ( $\rho = 0.1 \text{ fm}^{-3}$ ) (see the right panel (b) of Fig. 4), although the correlations are still opposite. We emphasize that these qualitative features emerge whatever the starting parameterization of the RMF or SHF model used.

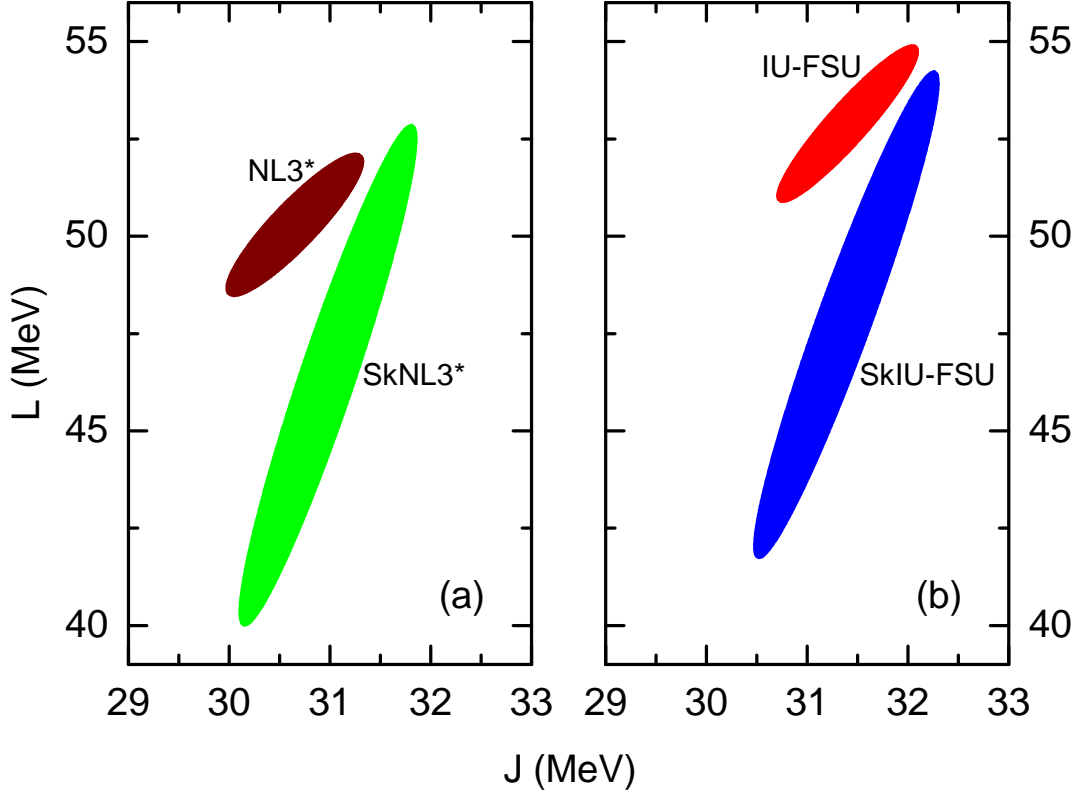


FIG. 3: (Color online)  $1\sigma$  joint confidence regions for the symmetry energy  $J$  and its slope parameter  $L$  at saturation density for the RMF and SHF models.

It is widely accepted that the Giant Monopole Resonance (GMR) provides the cleanest and most direct route to the nuclear incompressibility around normal density [62]. It has been also proposed that GMR energies of finite nuclei as well as the nuclear matter incompressibility should be computed within the same theoretical framework [63, 64]. The expression for the incompressibility of neutron-rich matter at saturation density is given by [62]:

$$K_{\text{sat}}(\alpha) = K_0 + K_\tau \alpha^2 + \mathcal{O}(\alpha^4), \quad (16)$$

where the coefficient of  $\alpha^2$  is

$$K_\tau = K_{\text{sym}} - 6L - \frac{Q_0}{K_0} L \quad (17)$$

with  $Q_0$  being the skewness of SNM [54]. Although both RMF and SHF models used in this work share the same value of  $K_0$ , their predictions of  $K_{\text{sat}}$  are different due to the difference in  $K_\tau$ , which in turn is mainly due to the difference in  $K_{\text{sym}}$ . In Table III we provide the values of  $K_{\text{sat}}$  for different values of isospin asymmetry. Due to the



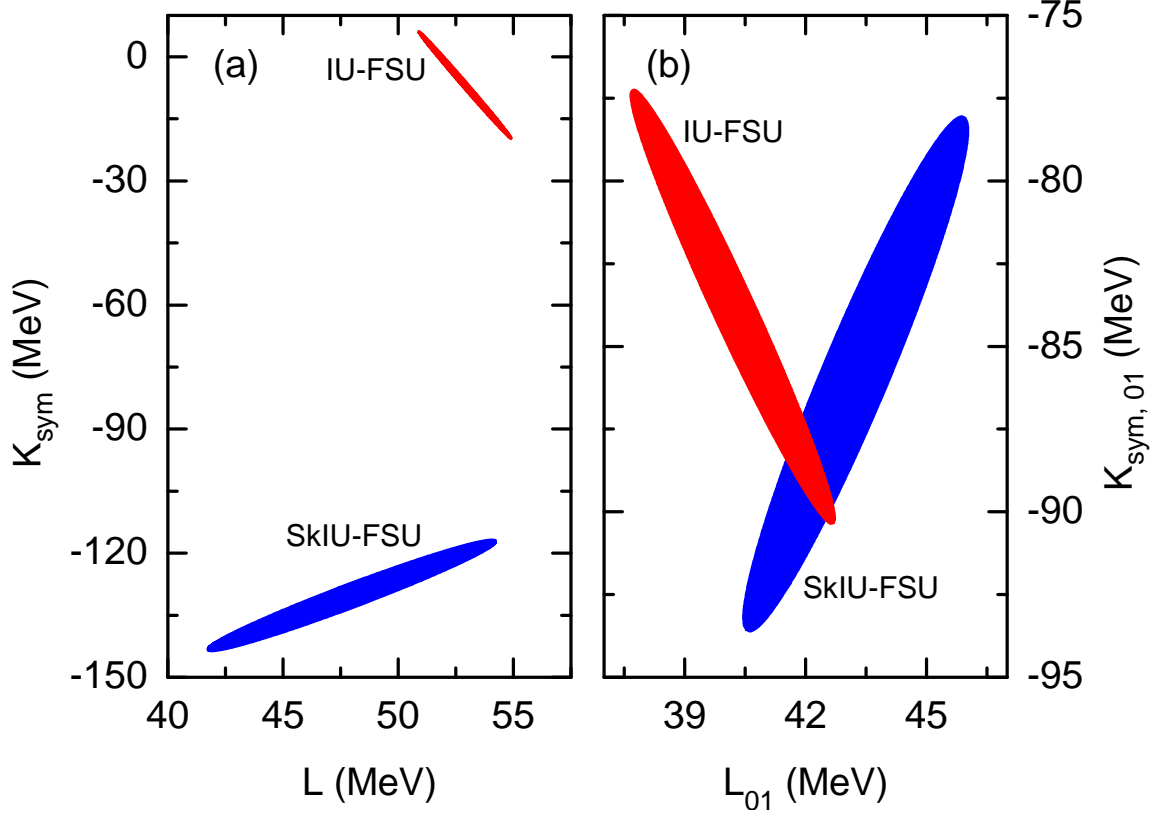


FIG. 4: (Color online)  $1\sigma$  joint confidence regions for the slope parameter  $L$  and curvature parameter  $K_{\text{sym}}$  of the symmetry energy at saturation density (a) and at  $\rho = 0.1 \text{ fm}^{-3}$  (b) from the IU-FSU and SkIU-FSU parameterizations.

small values of isospin asymmetry in finite nuclei, the difference of the incompressibility for different models is in fact small. Comparing with the constraint of  $-760 < K_\tau < -372 \text{ MeV}$  in Ref. [35] extracted directly from the GMR data, both RMF and SHF models predict marginally consistent or slightly higher values of  $K_\tau$  after the PNM optimization as shown in Table II, suggesting that both RMF and SHF models have difficulty in simultaneously predicting GMR properties consistent with experiment and the PNM EoS consistent with our best theoretical calculations.

	$K_{\text{sat}}(\alpha = 0) \text{ (MeV)}$	$K_{\text{sat}}(\alpha = 0.111) \text{ (MeV)}$	$K_{\text{sat}}(\alpha = 0.212) \text{ (MeV)}$
NL3*	258.5	255.0	245.8
SkNL3*	258.5	253.8	241.5
IU-FSU	231.3	228.2	219.8
SkIU-FSU	231.3	227.1	215.9

TABLE III: Incompressibility of neutron-rich matter with different isospin asymmetries  $\alpha = 0$  (SNM), 0.111 ( $^{90}\text{Zr}$ ), and 0.212 ( $^{208}\text{Pb}$ ) at saturation density from the four parameterizations after the PNM optimization.

Different values of the bulk properties of SNM will affect the PNM constraints on the symmetry energy. For example, the saturation density  $\rho_0$ , the binding energy at saturation  $E_0$ , and the incompressibility coefficient at saturation  $K_0$  will affect the EoS of SNM and thus modify slightly the optimized symmetry energy from a fixed set of PNM EoS constraints. The effective mass  $M^*$  dominates these uncertainties in the results of the PNM optimization. As can be seen from the expression for the symmetry energy in the RMF model [65]:

$$S(\rho) = \frac{k_F^2}{6\sqrt{k_F^2 + M^{*2}}} + \frac{g_\rho^2 \rho}{8m_\rho^{*2}}, \quad \left(m_\rho^{*2} \equiv m_\rho^2 + 2\Lambda_v g_\rho^2 (g_v V_0)^2\right) \quad (18)$$

$M^*$  affects the kinetic contribution to the symmetry energy while adjusting  $g_\rho$  and  $\Lambda_v$  only modifies the potential

	$J$ (MeV)	$L$ (MeV)	$K_\tau$ (MeV)
RMF	30.2 — 31.4	36.1 — 59.3	-329.7 — -215.7
SHF	30.1 — 33.2	28.5 — 64.4	-418.8 — -235.3

TABLE IV: Predicted ranges for symmetry energy parameters within RMF and SHF models with their pure isovector parameters optimized to PNM and taking into account all remaining variation from parameterizations constructed since 1995.

contribution to the symmetry energy. We find that increasing the effective mass at saturation by  $\sim 10\%$  decreases the optimized value of the slope of the symmetry energy at saturation density  $L$  by  $\sim 10$  MeV. The isovector effective mass, here set equal to the isoscalar effective mass in the SHF model to be consistent with the RMF models, affects the value of  $L$  obtained in the PNM optimization by the same order of magnitude, but in the opposite direction. The curvature of the symmetry energy  $K_{\text{sym}}$  is changed by a much smaller relative amount. Therefore the  $1\text{-}\sigma$  confidence ellipses change their positions in the  $J$ - $L$  plane as the SNM properties are varied, but they retain very similar values of their slopes, and the RMF and SHF confidence ellipses maintain their relative positions. Similarly, the  $K_{\text{sym}}$ - $L$  confidence ellipses change their  $L$ -position upon variation of SNM properties, but retain their  $K_{\text{sym}}$  values and relative orientation and spacing.

In order to get a better idea of the overall range of predictions for  $J$ ,  $L$  and  $K_\tau$  taking the additional model parameters into account, we take 11 RMF parameterizations and 73 SHF parameterizations from the literature that have been created since 1995 [35, 36]. We optimize the pure isovector parameters of each parameterization to the PNM results and examine the resultant constraints; these are displayed in Table IV.

### C. Implications for predictions of neutron skin thicknesses and neutron star radii

Measurements of the neutron skin thicknesses of various nuclides using strong interaction probes [4, 66–74] and, recently, weak interaction probes [75, 76] in the PREX experiment, are an important tool to probe the density dependence of the symmetry energy due to the very close correlation of  $L$  to the size of the neutron skin in neutron-rich nuclides [7, 41, 77–79]. Since our optimized RMF and SHF models give nearly matching ranges of  $L$ , we expect the neutron skin predictions to be similar.

In Fig. 5, we compare predictions of neutron skin thicknesses from the IU-FSU and SkIU-FSU parameterizations to the currently existing data on the neutron skin thickness of Tin isotopes [4, 67, 71–74]. As expected, both the post-optimization IU-FSU and SkIU-FSU models agree well with the experimental data, with the RMF model giving a systematically slightly higher value than the SHF model in all but the lightest isotopes calculated. Thus consistency with our best knowledge of the PNM EoS can be achieved simultaneously with consistency of neutron skin predictions with current experimental data within the RMF and SHF models.

The IU-FSU parameterization predicts  $R_{\text{skin}} = 0.18 \pm 0.01$  fm for  $^{208}\text{Pb}$ , while SkIU-FSU predicts a slightly lower value of  $R_{\text{skin}} = 0.16 \pm 0.01$  fm (Table II). The smaller value of  $R_{\text{skin}}$  for SkIU-FSU is primarily due to model dependence, which leads to a smaller value of optimized  $L$  from the PNM constraints. The current PREX obtained value for the neutron skin thickness of lead is  $R_{\text{skin}} = 0.33^{+0.16}_{-0.18}$  fm [75]. If the new PREX experiment reduces the error bars without moving the central value for the neutron skin, almost all current models of the nuclear structure would need to be modified. Also, this would appear to call for a significant modification of the PNM microscopic calculations.

Finally, we examine how the different symmetry energy characteristics of RMF and SHF models are manifest in neutron star radius predictions. Using our four post-optimization parameterizations, we apply the EoS of  $\beta$ -stable and charge neutral neutron star matter composed of neutrons, protons, electrons, and muons throughout the core of the star. For the very low density outer crust we use the BPS equation of state [80]. The equation of state of the inner crust is approximated by the polytropic equation of state of the form  $P = A\mathcal{E}^{4/3} + B$  [81], where  $A$  and  $B$  are determined to match the EoS at the boundaries of the inner crust. Using our equations of state, we integrate the general relativistic equation for hydrostatic equilibrium (the Tolman-Oppenheimer-Volkoff equation) from the center to the surface of the star.

The reference RMF and SHF parameterizations before the PNM optimization predict a wide range of results for low mass neutron star radii as shown in the left panel (a) of Fig. 6. In particular, for a 1.0 solar mass neutron star the difference in the predictions of radii for the NL3\* and IU-FSU equations of state is equal to  $\Delta R_{1.0} \approx 2.8$  km. There is a similar difference between the original SkNL3\* and SkIU-FSU equation of state predictions, i.e.,  $\Delta R_{1.0} \approx 2.5$  km. This can be mainly attributed to the density dependence of the symmetry energy, which is quite different in the two parameterizations. Once calibrated to the PNM results, this difference almost vanishes within the same model as shown in the right panel (b) of Fig. 6, i.e., both RMF and SHF parameterizations now match each other more

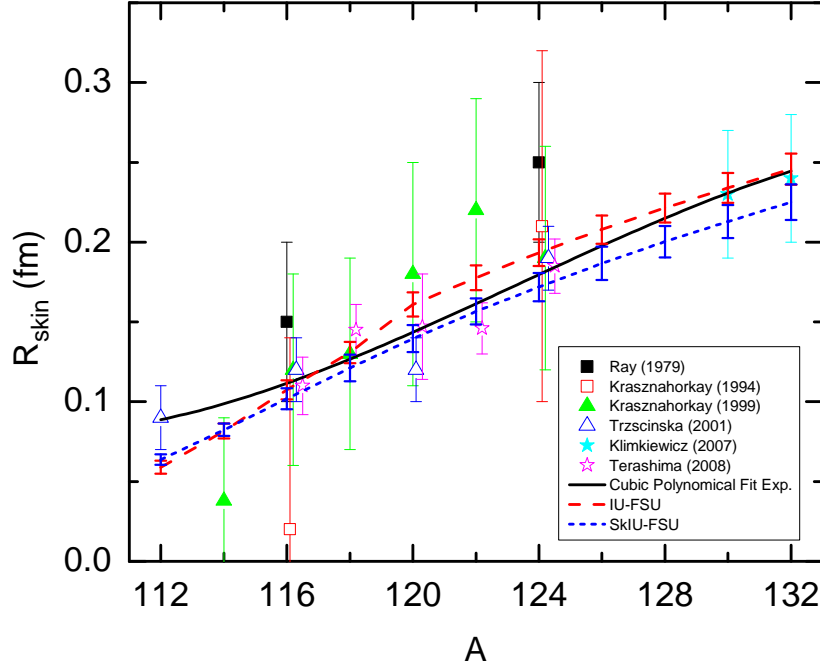


FIG. 5: (Color online) Comparing the predictions of the neutron skin thickness for Sn isotopes from the IU-FSU and SkIU-FSU models after the PNM optimization with those from different experimental methods.

closely (excepting the differences at high masses between the RMF models, a result of a stiffer EoS of SNM in NL3\* parameterizations at several times saturation density due to the  $\zeta$  parameter). Although both NL3\* and IU-FSU parameterizations in a given RMF or SHF model predict similar radii, there is a clear difference between the RMF and the SHF predictions as a whole. In the case of IU-FSU and SkIU-FSU we have almost a  $\sim 1$  km difference for the radius of a canonical neutron star. This discrepancy is even larger in the case of NL3\*, which is about  $\sim 1.8$  km. Thus, there is a strong model dependence when the two models are applied to neutron star structure calculations after the same PNM optimization.

The above model dependence actually comes from different density dependence of symmetry energy at supra-saturation densities, flagged by the model dependent difference in predictions of the curvature of the symmetry energy at saturation density  $K_{\text{sym}}$ . In Fig. 7 we plot the density dependence of the symmetry energy for the RMF and SHF models under consideration after the PNM optimization. Note that the symmetry energy is almost the same in all the models up to  $\sim 1.5\rho_0$  saturation density. However, the symmetry energy in the RMF functional is a monotonic increasing function of density, while the SHF functional tends to give a decreasing symmetry energy with increasing density at higher densities. Again, this property is generic once the model has been optimized to PNM EoS. The reason for this difference is manifest in the functional forms of the symmetry energy given as:

$$S_{\text{RMF}}(\rho) = A(\rho)\rho^{2/3} + B(\rho)\rho, \quad (19)$$

$$S_{\text{SHF}}(\rho) = a\rho^{2/3} - b\rho - c\rho^{5/3} - d\rho^{\sigma+1}, \quad (20)$$

where  $A(\rho)$  and  $B(\rho)$  are positive-valued functions of density [see Eq. (18)],  $a \equiv \frac{\hbar^2}{6M} \left(\frac{3\pi^2}{2}\right)^{2/3}$  and  $b, c, d$  are constants that depend on Skyrme parameters only. The symmetry energy in the RMF model is always positive as given in Eq. (19), while certain terms of the symmetry energy in the SHF model can become negative at higher densities [see Eq. (20)].

Recently, it was shown that currently available neutron star mass and radius measurements provide significant constraints on the EoS of PNM all the way up to several saturation densities [82]. While this is true, we also show that the low-density PNM constraints alone result in a pronounced model dependency of radius predictions, as different masses and radii can be obtained with the similar saturation properties constrained by the low-density PNM EoS. Although our PNM optimization tightly constrains the symmetry energy up to a little above the saturation density,

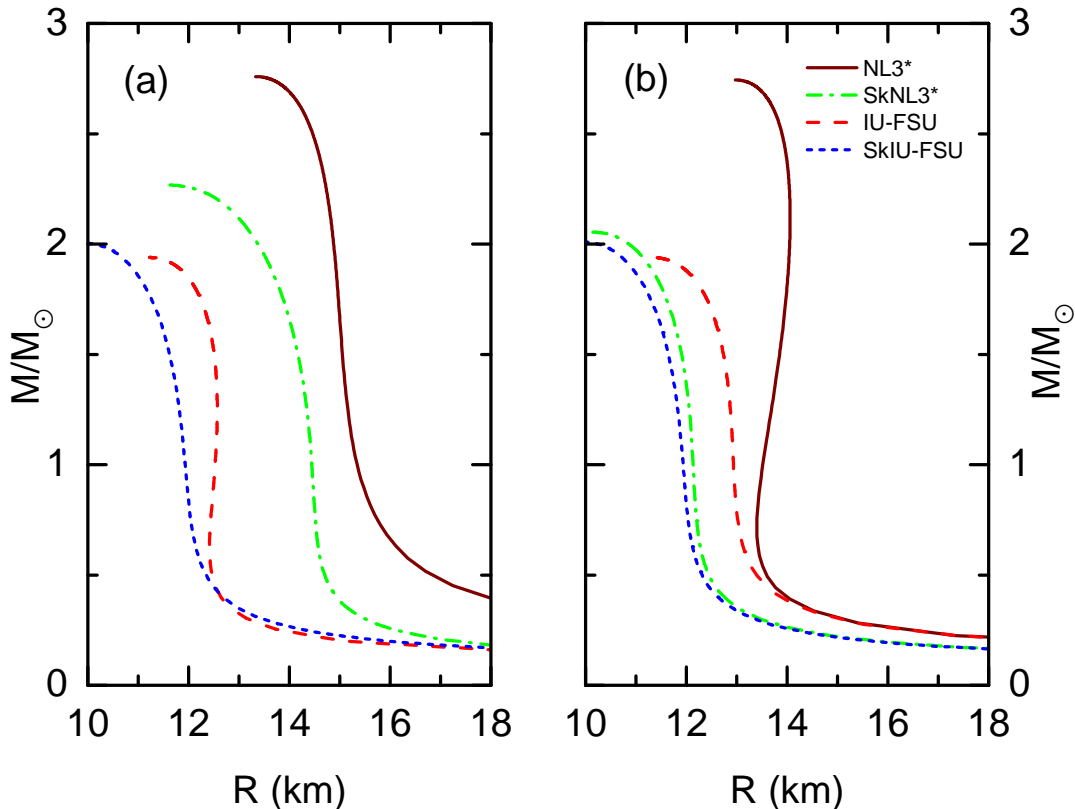


FIG. 6: (Color online) Mass-Radius relation of neutron stars calculated from the four parameterizations before (a) and after (b) the PNM optimization.

in order to understand its behavior at higher densities, which is also important in determining neutron star radii, one must rely on the heavy-ion collision experiments [83–85] and neutron star observations [86, 87].

#### IV. CONCLUSIONS

Using parameterizations of RMF and SHF energy-density functionals prepared to give equally good fits to ground state properties of doubly magic nuclei and identical symmetric nuclear matter properties, and are fit to state-of-the-art *ab initio* theoretical calculations of PNM up to saturation density, we have conducted a systematic examination of the resultant predictions from both models of the symmetry energy as a function of density and some important terrestrial nuclear and neutron star observables sensitive to  $S(\rho)$ .

We show that such RMF and SHF models result in very similar predictions for the symmetry energy  $J$  and its slope parameter  $L$  at saturation density from both models so long as the isoscalar effective mass from the SHF model is chosen to be equal to the Lorentz effective mass from the RMF model, which is tightly constrained around  $\approx 0.7M$ . Both models then give  $J \approx 31.0 \pm 1$  MeV. The SHF parameterizations give values around  $46 - 49 \pm 6$  MeV and the RMF parameterizations  $50 - 53 \pm 2$  MeV for  $L$ . Resulting predictions of neutron skin thicknesses  $R_{\text{skin}}$  for Sn isotopes and  $^{208}\text{Pb}$  therefore agree closely and are consistent with the available experimental data.

When the  $1\sigma$  error bounds are plotted as ellipses in the  $J$ - $L$  plane, a positively-correlated relationship between  $J$  and  $L$  is observed for both models. However, different slopes are obtained from the RMF and SHF models, and the two ellipses have no overlapping area in the plane. This model dependence comes from the different values of  $K_{\text{sym}}$  and higher-order symmetry energy parameters; i.e. from the different functional form of the symmetry energy implicit in the models. Although the PNM constraints lead to broadly similar behaviors of the symmetry energy as a function of density up to  $\approx 1.5\rho_0$ , they deviate significantly at higher densities due to the differences in the functional form of the symmetry energy. With the same PNM constraints up to the saturation density, the RHF model tends to predict a rising symmetry energy at higher densities, whereas the SHF model predicts a symmetry energy that may decrease

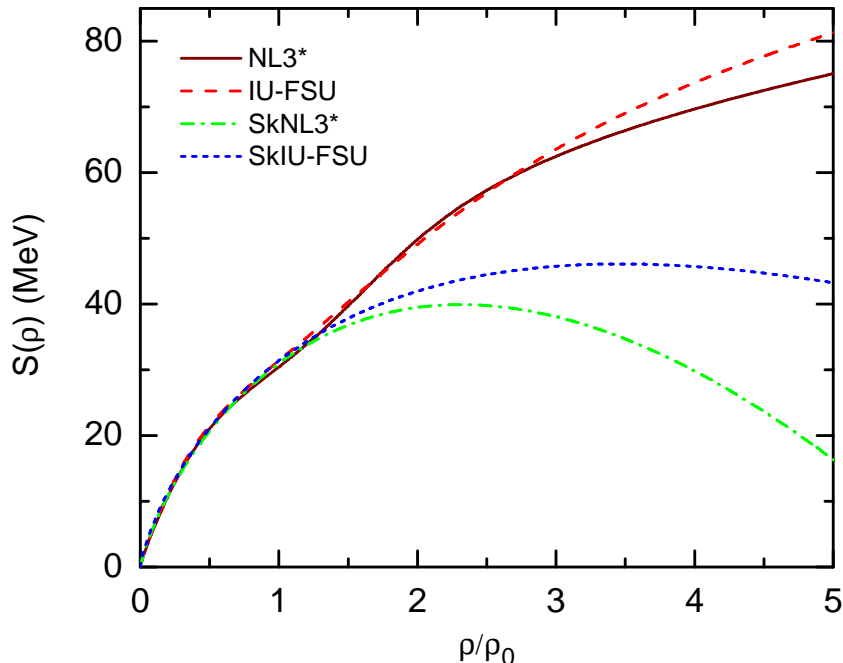


FIG. 7: (Color online) Density dependence of symmetry energy from the four parameterizations after the PNM optimization.

with density at higher densities, and thus leading to the uncertainty of up to  $\sim 2$  km in neutron star radii. Care must therefore be taken in extracting constraints on the symmetry energy, particularly on  $J$  and  $L$ , from inferred neutron star radii within one particular model.

The absolute values of the predictions are found to be mainly sensitive to the effective mass, with increases (decreases) of  $\sim 0.1 M$  leading to decreases (increases) of  $L$  by  $\sim 10$  MeV. We confirm this systematic analysis by analyzing the predictions from 11 RMF and 73 SHF parameterizations constructed since 1995, finding overall ranges taking into account remaining freedom in the parameter values, of  $30 \lesssim J \lesssim 31.5$  MeV,  $35 \lesssim L \lesssim 60$  MeV,  $-330 \lesssim K_\tau \lesssim -216$  MeV for RMF models and  $30 \lesssim J \lesssim 33$  MeV,  $28 \lesssim L \lesssim 65$  MeV,  $-420 \lesssim K_\tau \lesssim -325$  for SHF models.

Notably, some recent constraints inferred from experimental data on giant monopole resonances of Sn and Cd isotopes [40, 88, 89] and on neutron skins [7] place  $K_\tau$  in the overall range  $-650 < K_\tau < -375$  MeV. It has been pointed out that these results are inconsistent with many individual Skyrme parameterizations and microscopic nuclear matter calculations [35, 39]; our results generalize these points to demonstrate that these particular  $K_\tau$  constraints are inconsistent with the RMF model as a whole and only marginally consistent with SHF models as a whole, within  $1\sigma$  confidence intervals resulting from optimization to PNM calculations. Thus, either the density dependence of RMF and SHF models is insufficient to simultaneously describe PNM within current bounds and GMR/neutron skin experimental data, or there are overlooked problems with the extraction of the  $K_\tau$  constraints in the above works and the error bounds are underestimated, as has been suggested [39]. Note that the  $K_\tau$  ranges we extract from both models are consistent with another  $K_\tau$  constraint extracted from isospin diffusion in heavy ion collisions  $-490 < K_\tau < -250$  MeV [54]. More work needs to be done to check these hypotheses while taking the dependency of functional forms (e.g. [90]) into consideration.

### Acknowledgments

The authors are grateful to Prof. Lie-Wen Chen for providing the experimental data of neutron skin thickness of Tin isotopes, to Dr. Stefano Gandolfi for making available the AFDMC data, and to Prof. Jorge Piekarewicz for providing the Hartree code to calculate the ground state properties of finite nuclei in the RMF model, and for many fruitful discussions. This work is supported in part by the National Aeronautics and Space Administration under

grant NNX11AC41G issued through the Science Mission Directorate, and the National Science Foundation under Grants No. PHY-1068022 and No. PHY-0757839.

- 
- [1] L.-W. Chen, C. M. Ko, and B.-A. Li, Phys. Rev. Lett. **94**, 032701 (2005).
  - [2] M. Famiano *et al.*, Phys. Rev. Lett. **97**, 052701 (2006).
  - [3] D. V. Shetty, S. J. Yennello, and G. A. Souliotis, Phys. Rev. **C76**, 024606 (2007).
  - [4] A. Klimkiewicz *et al.*, Phys. Rev. **C76**, 051603 (2007).
  - [5] P. Danielewicz and J. Lee, Nucl. Phys. **A818**, 36 (2009).
  - [6] M. B. Tsang, Yingxun Zhang, P. Danielewicz, M. Famiano, Zhuxia Li, W. G. Lynch, and A. W. Steiner, Phys. Rev. Lett. **102**, 122701 (2009).
  - [7] M. Centelles, X. Roca-Maza, X. Vinas, and M. Warda, Phys. Rev. Lett. **102**, 122502 (2009).
  - [8] M. Warda, X. Vinas, X. Roca-Maza, and M. Centelles, Phys. Rev. **C80**, 024316 (2009).
  - [9] A. Carbone, G. Colò, A. Bracco, L.-G. Cao, P. F. Bortignon, F. Camera, and O. Wieland, Phys. Rev. **C81**, 041301 (2010).
  - [10] L.-W. Chen, C. M. Ko, B.-A. Li, and J. Xu, Phys. Rev. **C82**, 024321 (2010).
  - [11] J. Zenihiro *et al.*, Phys. Rev. **C82**, 044611 (2010).
  - [12] C. Xu, B.-A. Li, and L.-W. Chen, Phys. Rev. **C82**, 054607 (2010).
  - [13] M. Liu, N. Wang, Z.-X. Li, and F.-S. Zhang, Phys. Rev. **C82**, 064306 (2010).
  - [14] L.-W. Chen, Phys. Rev. **C83**, 044308 (2011).
  - [15] P. Möller, W. D. Myers, H. Sagawa, and S. Yoshida, Phys. Rev. Lett. **108**, 052501 (2012).
  - [16] J. M. Lattimer and Y. Lim (2012), 1203.4286.
  - [17] J. Dong, W. Zuo, J. Gu, and U. Lombardo, Phys. Rev. **C85**, 034308 (2012).
  - [18] J. Piekarewicz, B. K. Agrawal, G. Colò, W. Nazarewicz, N. Paar, P.-G. Reinhard, X. Roca-Maza, and D. Vretenar, Phys. Rev. **C85**, 041302 (2012).
  - [19] M. Tsang *et al.* Phys. Rev. **C86**, 015803 (2012).
  - [20] B.-A. Li *et al.*, J. Phys. Conf. Ser. **312**, 042006 (2011).
  - [21] A. Schwenk and C. J. Pethick, Phys. Rev. Lett. **95**, 160401 (2005).
  - [22] A. Gezerlis and J. Carlson, Phys. Rev. **C81**, 025803 (2010).
  - [23] A. Gezerlis and J. Carlson (2011), 1109.4946.
  - [24] K. Hebeler and A. Schwenk, Phys. Rev. **C82**, 014314 (2010).
  - [25] S. Gandolfi, A. Y. Illarionov, K. E. Schmidt, F. Pederiva, and S. Fantoni, Phys. Rev. **C79**, 054005 (2009).
  - [26] S. Gandolfi, A. Yu. Illarionov, S. Fantoni, J. C. Miller, F. Pederiva, and K. E. Schmidt, Mon. Not. Roy. Astron. Soc. **404**, L35 (2010).
  - [27] S. Gandolfi, J. Carlson, and S. Reddy, Phys. Rev. **C85**, 032801 (2012).
  - [28] *Building a universal nuclear energy density functional*, (UNEDF Collaboration), URL <http://unedf.org>.
  - [29] B. D. Serot and J. D. Walecka, Adv. Nucl. Phys. **16**, 1 (1986).
  - [30] B. D. Serot and J. D. Walecka, Int. J. Mod. Phys. **E6**, 515 (1997).
  - [31] T. Skyrme, Phil. Mag. **1**, 1043 (1956).
  - [32] D. Vautherin and D. Brink, Phys. Rev. **C5**, 626 (1972).
  - [33] P. Reinhard, Rept. Prog. Phys. **52**, 439 (1989).
  - [34] A. Sulaksono, T. Burvenich, J. Maruhn, P. Reinhard, and W. Greiner, Annals Phys. **308**, 354 (2003).
  - [35] M. Dutra, O. Lourenço, J. S. Sà Martins, A. Delfino, J. R. Stone, and P. D. Stevenson, Phys. Rev. **C85**, 035201 (2012).
  - [36] L.-W. Chen, C. M. Ko, and B.-A. Li, Phys. Rev. **C76**, 054316 (2007).
  - [37] P.-G. Reinhard and W. Nazarewicz, Phys. Rev. **C81**, 051303 (2010).
  - [38] F. J. Fattoyev and J. Piekarewicz, Phys. Rev. **C84**, 064302 (2011).
  - [39] J. M. Pearson, N. Chamel, and S. Goriely, Phys. Rev. **C82**, 037301 (2010).
  - [40] U. Garg, Acta Phys. Polon. **B42**, 659 (2011).
  - [41] I. Vidana, C. Providencia, A. Polls, and A. Rios, Phys. Rev. **C80**, 045806 (2009).
  - [42] H. Mueller and B. D. Serot, Nucl. Phys. **A606**, 508 (1996).
  - [43] B. G. Todd-Rutel and J. Piekarewicz, Phys. Rev. Lett. **95**, 122501 (2005).
  - [44] G. A. Lalazissis, J. König, and P. Ring, Phys. Rev. **C55**, 540 (1997).
  - [45] G. A. Lalazissis, S. Raman, and P. Ring, At. Data Nucl. Data Tables **71**, 1 (1999).
  - [46] R. J. Furnstahl, B. D. Serot, and H.-B. Tang, Nucl. Phys. **A615**, 441 (1997).
  - [47] E. Chabanat, J. Meyer, P. Bonche, R. Schaeffer, and P. Haensel, Nucl. Phys. **A627**, 710 (1997).
  - [48] S. Brandt, *Data Analysis: Statistical and Computational Methods for Scientists and Engineers* (Springer, New York, 1999), 3rd ed.
  - [49] A. Akmal, V. R. Pandharipande, and D. G. Ravenhall, Phys. Rev. **C58**, 1804 (1998).
  - [50] K. Hebeler, J. M. Lattimer, C. J. Pethick, and A. Schwenk, Phys. Rev. Lett. **105**, 161102 (2010).
  - [51] C. J. Horowitz and J. Piekarewicz, Phys. Rev. Lett. **86**, 5647 (2001).
  - [52] G. A. Lalazissis, S. Karatzikos, R. Fossion, D. Pena Arteaga, A. V. Afanasjev, and P. Ring, Phys. Lett. **B671**, 36 (2009).
  - [53] F. J. Fattoyev, C. J. Horowitz, J. Piekarewicz, and G. Shen, Phys. Rev. **C82**, 055803 (2010).

- [54] L.-W. Chen, B.-J. Cai, C. M. Ko, B.-A. Li, C. Shen, and J. Xu, Phys. Rev. **C80**, 014322 (2009).
- [55] E. N. E. van Dalen, C. Fuchs, and A. Faessler, Phys. Rev. Lett. **95**, 022302 (2005).
- [56] Y. Gambhir, P. Ring, and A. Thimet, Annals Phys. **198**, 132 (1990).
- [57] A. Bodmer, Nucl. Phys. **A526**, 703 (1991).
- [58] R. J. Furnstahl, J. J. Rusnak, and B. D. Serot, Nucl. Phys. **A632**, 607 (1998).
- [59] M. Jaminon and C. Mahaux, Phys. Rev. **C40**, 354 (1989).
- [60] G. Audi, A. H. Wapstra, and C. Thibault, Nucl. Phys. **A729**, 337 (2002).
- [61] I. Angeli, At. Data Nucl. Data Tables **87**, 185 (2004).
- [62] J. Piekarewicz and M. Centelles, Phys. Rev. **C79**, 054311 (2009).
- [63] J. P. Blaizot, Phys. Rept. **64**, 171 (1980).
- [64] J. P. Blaizot, J. F. Berger, J. Dechargé, and M. Girod, Nucl. Phys. **A591**, 435 (1995).
- [65] C. J. Horowitz and J. Piekarewicz, Phys. Rev. **C64**, 062802 (2001).
- [66] L. Ray, W. R. Coker, and G. W. Hoffmann, Phys. Rev. **C18**, 2641 (1978).
- [67] L. Ray, Phys. Rev. **C19**, 1855 (1979).
- [68] C. Garcia-Recio, J. Nieves, and E. Oset, Nucl. Phys. **A547**, 473 (1992).
- [69] V. E. Starodubsky and N. M. Hintz, Phys. Rev. **C49**, 2118 (1994).
- [70] B. C. Clark, L. J. Kerr, and S. Hama, Phys. Rev. **C67**, 054605 (2003).
- [71] A. Trzcińska, J. Jastrzębski, P. Lubiński, F. J. Hartmann, R. Schmidt, T. von Egidy, and B. Klos, Phys. Rev. Lett. **87**, 082501 (2001).
- [72] A. Krasznahorkay, A. Balanda, J. A. Bordewijk, S. Brandenburg, M. N. Harakeh, N. Kalantar-Nayestanaki, B. M. Nyako, J. Timar, and A. van der Woude, Nucl. Phys. **A567**, 521 (1994).
- [73] A. Krasznahorkay *et al.*, Phys. Rev. Lett. **82**, 3216 (1999).
- [74] S. Terashima *et al.*, Phys. Rev. **C77**, 024317 (2008).
- [75] S. Abrahamyan *et al.*, Phys. Rev. Lett. **108**, 112502 (2012).
- [76] S. Ban, C. Horowitz, and R. Michaels, J. Phys. G **39**, 015104 (2012).
- [77] B. A. Brown, Phys. Rev. Lett. **85**, 5296 (2000).
- [78] R. J. Furnstahl, Nucl. Phys. **A706**, 85 (2002).
- [79] M. Centelles, X. Roca-Maza, X. Vinas, and M. Warda, Phys. Rev. **C82**, 054314 (2010).
- [80] G. Baym, C. Pethick, and P. Sutherland, Astrophys. J. **170**, 299 (1971).
- [81] J. Carriere, C. J. Horowitz, and J. Piekarewicz, Astrophys. J. **593**, 463 (2003).
- [82] A. W. Steiner and S. Gandolfi, Phys. Rev. Lett. **108**, 081102 (2012).
- [83] P. Danielewicz, R. Lacey, and W. G. Lynch, Science **298**, 1592 (2002).
- [84] B.-A. Li, L.-W. Chen, and C. M. Ko, Phys. Rept. **464**, 113 (2008).
- [85] V. Baran, M. Colonna, V. Greco, and M. Di Toro, Phys. Rept. **410**, 335 (2005).
- [86] J. M. Lattimer and M. Prakash, Phys. Rept. **442**, 109 (2007).
- [87] A. W. Steiner, M. Prakash, J. M. Lattimer, and P. J. Ellis, Phys. Rept. **411**, 325 (2005).
- [88] T. Li *et al.*, Phys. Rev. Lett. **99**, 162503 (2007).
- [89] H. Sagawa, S. Yoshida, G.-M. Zeng, J.-Z. Gu, and X.-Z. Zhang, Phys. Rev. **C76**, 034327 (2007).
- [90] J. Erler, P. Klupfel, and P.-G. Reinhard, Phys. Rev. **C82**, 044307 (2010).